THE ASTRONOMICAL JOURNAL, 122:2099–2114, 2001 October
© 2001. The American Astronomical Society. All rights reserved. Printed in U.S.A.

COLORS AND SPECTRA OF KUIPER BELT OBJECTS[1]

DAVID C. JEWITT[2]
Institute for Astronomy, 2680 Woodlawn Drive, Honolulu, HI 96822

AND

JANE X. LUU
Leiden Observatory, Postbus 9513, NL-2300 RA Leiden, Netherlands
Received 2001 May 14; accepted 2001 July 10

ABSTRACT

We present new measurements of the optical colors of Kuiper belt objects, principally from the Keck 10 m telescope. The measurements confirm the existence of a wide spread in the $B-V$, $V-R$, and $R-I$ color indices as we found previously. Relative to the sun, the Kuiper belt objects exhibit reflected colors from nearly neutral to very red. The optical and optical-infrared ($V-J$) color indices are mutually correlated, showing the presence of a single reddening agent from 0.45 to 1.2 μm. On the other hand, we find no evidence for linear correlations between the color and absolute magnitude (a proxy for size), instantaneous heliocentric distance, semimajor axis, or with any other orbital property. In this regard, the Kuiper belt objects differ from the main-belt asteroids, in which strong radial color gradients exist. We find no statistically significant evidence for bimodal or other nonuniform color distributions, either in our data or in data previously reported to show such evidence. The impact resurfacing hypothesis is reexamined in the light of the new color data and is rejected as the primary cause of the observed color dispersion. We also present new near-infrared reflection spectra of 1993 SC, 1996 TS_{66}, 1999 DE_9 and 2000 EB_{173}, taken at the Keck and Subaru telescopes. These spectra, combined with others from the published literature, provide independent evidence for compositional diversity in the Kuiper belt. Objects 2000 EB_{173}, 1993 SC, and 1996 TS_{66} are spectrally bland, while 1999 DE_9 shows solid-state absorption bands.

Key words: comets: general — Kuiper belt — solar system: formation

1. INTRODUCTION

Ground-based surveys have revealed (as of 2001 July) more than 400 Kuiper belt objects (KBOs). These bodies have orbital semimajor axes $a > 30$ AU and a wide range of orbital properties showing clear evidence for dynamical substructuring (Jewitt, Luu, & Chen 1996; Luu et al. 1997; Jewitt, Luu, & Trujillo 1998; Trujillo, Jewitt, & Luu 2000). The inferred population of objects with diameters ≥ 100 km is of order 4×10^4 (in the classical belt; Trujillo, Jewitt, & Luu 2001), while the inferred number of (mostly unseen) bodies larger than 1 km in diameter amounts to many billions.

The Kuiper belt is thought to be a relic from the earliest phases of the solar system. The low radiation equilibrium temperatures of KBOs ($T \approx 40$–50 K) allow the possibility that many common ices could be retained over the age of the solar system. Indeed, it is widely thought that the volatile-rich nuclei of most short-period (specifically, Jupiter-family) comets are escaped members of the Kuiper belt, while the Centaurs (bodies with perihelia and semimajor axes between the orbits of Jupiter and Neptune) represent an intermediate dynamical stage. There is strong interest in understanding the physical properties and compositional natures of the KBOs, both as clues to the early solar system and as samples of cometary material relatively unchanged by heating by the Sun. Unfortunately, most known KBOs are faint (apparent red magnitude $m_R \geq 22$), and their properties are difficult to measure with accuracy. The most secure and, so far, uncontested observational result is that the KBOs exhibit diverse optical colors ranging from nearly neutral ($V-R \approx 0.3$) to very red ($V-R \approx 0.7$–0.8) (Luu & Jewitt 1996; Green et al. 1997; Tegler & Romanishin 1998; Barucci et al. 2000). A wide range in the $V-J$ color index also appears to be well established (Jewitt & Luu 1998; Davies et al. 2000; Noll, Luu, & Gilmore 2000).

Two qualitative explanations for the color diversity of KBOs have been proposed (Luu & Jewitt 1996). First, color differences might result from the competition between cosmic-ray bombardment (which may tend to produce a low-albedo, reddish reflectivity) and occasional impact excavation of subsurface volatiles. The resurfacing hypothesis makes specific predictions about the color distribution of the KBOs and is therefore testable. Resurfacing is only effective as a cause of spectral diversity when the timescales for irradiation darkening and impact resurfacing are comparable. The resulting surfaces of the KBOs should occupy a continuum of states from fully mantled, low albedo, and reddish at one end to fully resurfaced, ice covered, and neutral at the other. Furthermore, since not all resurfacing events would globally coat KBOs with excavated material, a second prediction is that the colors (and spectra) of KBOs should be azimuthally variable. A third prediction is that the rotationally averaged colors of the KBOs should systematically vary with the object size, since small bodies have shorter resurfacing times than larger ones, while the cosmic-ray reddening timescale is independent of size (see Fig. 4 of Luu & Jewitt 1996).

[1] Based in part on data collected at the Subaru Telescope, which is operated by the National Astronomical Observatory of Japan.

[2] Visiting Astronomer, W. M. Keck Observatory, which is operated as a scientific partnership among the California Institute of Technology, the University of California, and the National Aeronautics and Space Administration. The Observatory was made possible by the generous financial support of the W. M. Keck Foundation.

Alternatively, color diversity could simply indicate intrinsically different compositions among the KBOs. This second hypothesis is difficult to reconcile with the relatively small temperature gradients expected across the trans-Neptunian solar system. In radiative equilibrium with the sun, the local blackbody temperature varies as $T(R) \approx 278R^{-1/2}$, where R (AU) is the heliocentric distance. The temperature difference from 30 to 50 AU is a paltry 11 K, scarcely enough to affect the chemical composition of the KBOs. Slightly larger temperature gradients might be expected if the KBOs have been swept outward from their formation locations by the radial migration of Neptune, but still it is difficult to see how the bulk composition could be substantially affected. Nevertheless, in view of the uncertainties in the modes of formation and dynamical histories of the KBOs, the second hypothesis cannot yet be ruled out as a viable explanation of the color distributions of the KBOs.

Tegler & Romanishin (1998, 2000, hereafter TR98 and TR00) reported a bimodal distribution of KBO colors. Independently, Barucci et al. (2001) refute this bimodality but report evidence for four distinct color groups within the KBO population. Bimodal and multimodal distributions are interesting in the present context because they cannot be produced by stochastic resurfacing. The question of whether the KBO color distribution is unimodal or bimodal therefore confronts the resurfacing hypothesis. While a number of authors have published color measurements that specifically refute the bimodal distribution (Barucci et al. 2000; Davies et al. 2000), it is in fact difficult to imagine how such a distribution could be produced as an artifact. For example, low-quality photometry having large uncertainties will tend to blur a bimodal distribution into a unimodal one, not the other way round. This raises the possibility that Tegler & Romanishin's careful use of aperture correction techniques in photometry could be responsible for their detecting bimodality, while others do not see it (Barucci et al. 2000 used aperture correction, but their sample included only eight objects). We investigate this possibility in § 2.

In this paper, we present new optical photometry of 26 KBOs and two Centaurs taken at the Keck and University of Hawaii telescopes. The new measurements constitute a single data set relatively free of systematic errors that might afflict conclusions drawn by comparing photometry from different sources. In addition, we present new reflection spectra of four KBOs in the near-infrared (1 μm $\leq \lambda \leq$ 2.4 μm) wavelength range. We ask the following questions:

1. Are the optical colors bimodally distributed?
2. Are the optical and optical near-infrared colors correlated?
3. Are there correlations between surface color and physical or orbital properties of the KBOs?
4. Are the available data compatible with the resurfacing hypothesis?
5. What clues are provided by the spectral evidence?

2. OPTICAL OBSERVATIONS

Optical observations were obtained under photometric conditions at the Keck II telescope using the LRIS imaging camera (Oke et al. 1995). This camera incorporates a Tektronix 2048 × 2048 pixel charge-coupled device (CCD) and gives an image scale of 0.″215 per 24 μm pixel. Facility broadband *BVRI* filters were used for all observations. Photometric calibration of the data was obtained through observations of standard stars on the Johnson-Kron-Cousins photometric system (Landolt 1992). The images were processed using flat fields calculated from the nightly medians of bias-subtracted data taken through each filter. The resulting images were found to be uniform in sensitivity across the width of the CCD to better than 1%, with the largest deviations occurring near the east and west edges of the field of view in a region that was partially vignetted by the LRIS optics. All target objects and standard stars were placed within 300 pixels of the center of the field of view (FOV) and completely avoided the vignetting. The images were autoguided at sidereal rates. We used short integration times (from 200 to 500 s) in order to minimize trailing of the KBOs relative to the stars. At opposition, the KBOs trail ~0.″4 in 500 s, which is small compared with the 0.″7–1.″0 FWHM seeing in most of our data.

Additional optical observations of four bright KBOs were obtained at the University of Hawaii 2.2 m telescope. We used a Tektronix 2048 × 2048 pixel CCD camera at the f/10 Cassegrain focus to obtain a 7.5 × 7.5 arcmin^2 FOV and a 0.″219 pixel^{-1} image scale. Flat fielding and photometric calibration were obtained as at the Keck telescope.

2.1. *Profile Correction*

There are several sources of uncertainty in the photometry, and in view of the importance of the errors it seems worthwhile to discuss them here. The main problem is that, while large photometry apertures are needed to capture all the light in the point-spread function (PSF), large apertures also capture a large (and noisy) signal from the background sky. Specifically, if the function $f(a)$ (W m^{-2} Hz^{-1} arcsec^{-2}) represents the PSF, the total flux within the PSF measured out to radius a (arcsec) is simply

$$F(a) = \int_0^a 2\pi a f(a) da \,, \tag{1}$$

while the flux in the background measured out to the same radius is

$$F_b(a) = \int_0^a 2\pi a f_b \, da = \pi a^2 f_b \,, \tag{2}$$

where f_b (W m^{-2} Hz^{-1} arcsec^{-2}) is the sky surface brightness. Ideally, we would like to measure $F(a \rightarrow \infty)$ to capture all of the light from the PSF, but then background signal $F_b(a \rightarrow \infty) \rightarrow \infty$. For faint objects, the noise on the background sky completely dominates the photometric uncertainty. The tempting option is to use photometry from small apertures to reduce random errors caused by noise on the background signal. However, this introduces potentially devastating systematic errors due to the variable and unknown fraction of the total light captured within the small aperture.

We followed the example of TR98 and used photometry of field stars to empirically determine a profile correction, defined by

$$\Delta m_p = -2.5 \log \left[\frac{F(a_1)}{F(a_2)} \right] . \tag{3}$$

Here, a_1 and a_2 are the radii of the small and large photometry apertures used, respectively, to measure the

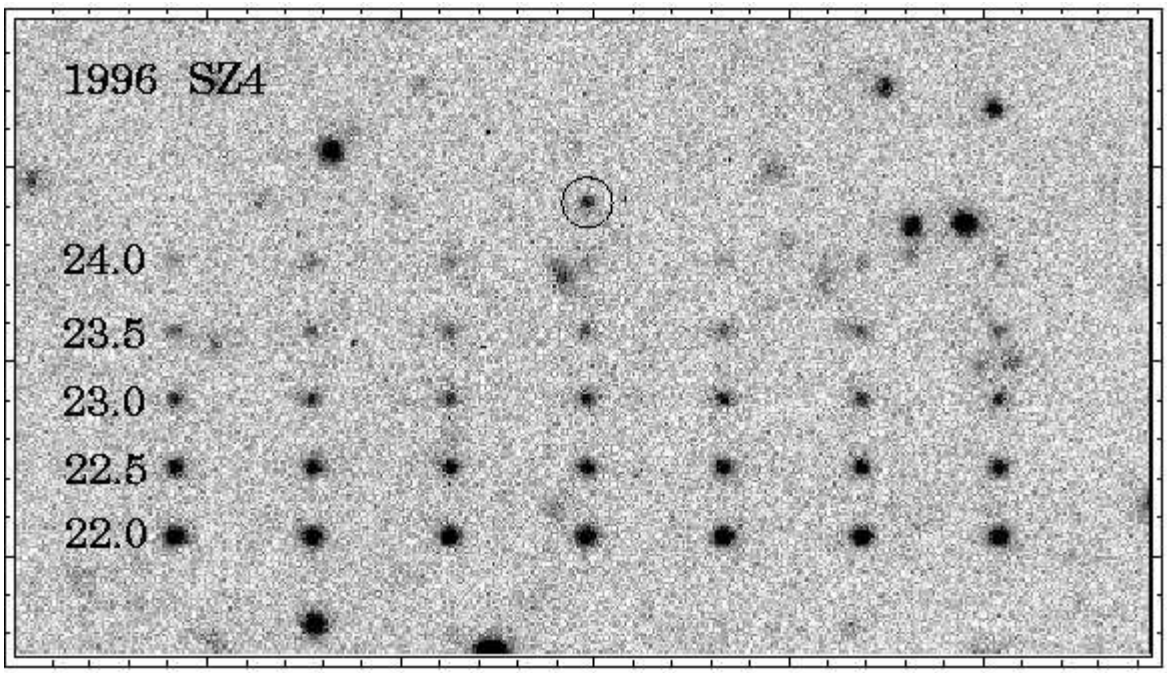

FIG. 1.—Keck image of 1996 SZ_4 (*circled*) with a grid of artificial images added to assess the noise properties of the data. The magnitudes of the synthesized images vary vertically in the figure, as marked. At each magnitude seven artificial images have been added to measure the effect of background fluctuations on the extracted photometry. This is a 300 s integration through the *R* filter, taken 1998 November 14.

KBOs and their reference field stars and the photometric standard stars. Essentially, equation (3) is a correction to be added to small-aperture measurements of KBO magnitudes to estimate the total flux density that would be obtained if low-noise, large-aperture measurements were possible. We experimented to determine optimal values of the aperture radii by trial and error, eventually selecting $a_1 = 1''.0$ and $a_2 = 3''.22$ for most measurements. The median sky signal was determined from a contiguous annulus $4''$ to $5''$ wide. Typically five to 10 field stars were identified in each image and used to determine Δm_p. In practice, we found two important limitations to this procedure. First, the PSF of the Keck data varies slightly with position on the CCD. We selected field stars near the target KBOs to reduce the effect of spatial variations. Second, in the fine seeing above Mauna Kea we could see that most of the field objects were marginally resolved galaxies, and in some fields we had difficulty locating a suitable number of stars with which to determine Δm_p. With the above parameters, we found $\Delta m_p = 0.3$ to 0.5 mag, depending on the seeing. The uncertainty in Δm_p determined from the dispersion among measurements of different field stars was typically $\sigma_p =$ 0.01–0.03 mag.

2.2. *Noise Properties of the Data*

We examined the effects of background fluctuations on the photometry by placing artificial KBOs on the CCD and measuring their magnitudes using procedures identical to those employed for real objects. The PSFs of the artificial KBOs were matched to the PSFs of the real data on an image-by-image basis, including allowance for nonzero ellipticity (e.g., caused by wind shake) where appropriate. Measurements of about 20 artificial objects were used to calculate the empirical standard deviation within each of several magnitude bins. A sample image is shown in Figure 1 for the particular case of 1996 SZ4. In background-limited observations, the photometric uncertainty σ_B should vary with the magnitude of the source m_R as

$$\sigma_B = -2.5 \log (1 + \kappa 10^{0.4 m_R}) , \quad (4)$$

where κ is a constant that depends on the surface brightness of the night sky and the integration time. We find that equation (4) provides an acceptable fit to the measurements in each filter (Fig. 2). The combined uncertainty is estimated from

$$\sigma = \sqrt{(\sigma_B^2 + \sigma_p^2)} . \quad (5)$$

The above error treatment accounts for contamination by background sources in a statistical sense. The photometry can potentially still suffer from contamination by

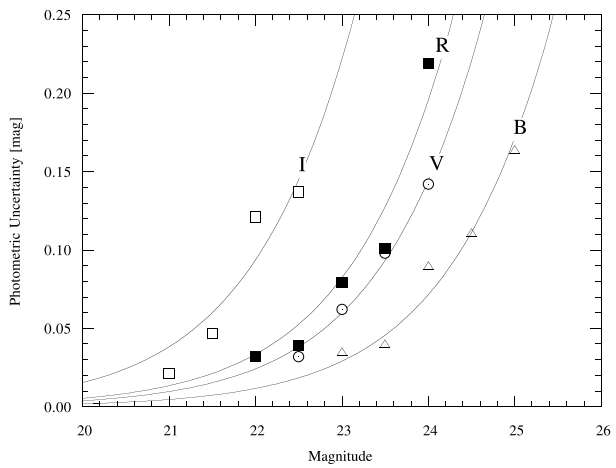

FIG. 2.—Sample photometric uncertainties as a function of apparent magnitude in the *BVR* and *I* filters for 300 s integrations, measured from simulations like the one in Fig. 1. The curves show eq. (4) fitted to the data.

rare, bright background sources that are not well sampled by the above procedure. Most such sources are distant galaxies, typically extended on scales comparable to the seeing. For example, a galaxy of red magnitude $m_R = 25$ constitutes a 2.5% (6.5%) error signal to a foreground KBO of magnitude $m_R = 21(22)$. We used the motion of KBOs between images to provide protection from such background objects. Photometry that was obviously compromised was rejected from the sample.

2.3. *Photometric Results*

The geometrical circumstances of the observations are summarized in Table 1. The optical photometry is listed in Table 2, while color-color plots are shown in Figures 3, 4, and 5. For reference, the corresponding colors of the Sun are approximately given by $B-V = 0.67$, $V-R = 0.36$, $R-I = 0.35$, $V-J = 1.08$ (Hartmann, Cruikshank, & Degewij 1982; Hartmann et al. 1990). The solar colors are marked in Figures 3 and 4. We note immediately from the figures that the $B-V$, $V-R$, and $R-I$ color indices are redder than the Sun and are mutually correlated: objects that are red at B (4500 Å wavelength) are also red at I (8500 Å). Linear correlation coefficients are summarized in Table 3. In the table, $P(r \geq r_{\rm corr})$ denotes the probability that a correlation coefficient equal to or larger than the one measured could be produced by chance in random, uncorrelated data. $P(r \geq r_{\rm corr}) = 0.003$ corresponds to the nominal 3 σ criterion for a statistically significant correlation.

The color-color correlations are extended to longer wavelengths in Figure 6, where we plot those objects

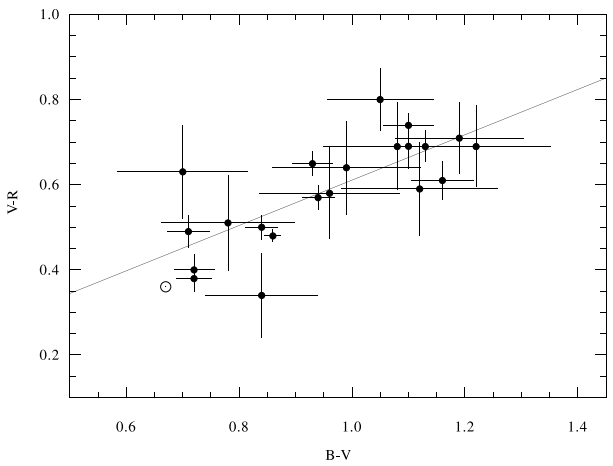

FIG. 3.—Plot of $B-V$ vs. $V-R$ for photometry from the present work having $\sigma_{B-V} < 0.15$ (see Table 2). The color of the Sun is marked. The least-squares fit is shown to guide the eye.

observed in J band (1.2 μm) from Jewitt & Luu (1998) and Davies et al. (2000). The $B-I$ and $V-J$ color indices are highly correlated (Table 3), suggesting that optical colors may be used as a proxy for the optical near-infrared $V-J$ color. The correlations show that the reflectivities of the KBOs are consistent with a single reddening agent in the B (0.45 μm) to J (1.2 μm) regime. Spectra of many low-albedo hydrocarbons show exactly this property (Cloutis, Gaffey, & Moslow 1994). The reflectivity gradients at wavelengths greater than 1.2 μm tend to be smaller, and they are not well

TABLE 1

GEOMETRICAL CIRCUMSTANCES OF THE OBSERVATIONS

Object	Class	Telescope	UT Date	R (AU)	D (AU)	α (deg)
Pluto	3:2	UH 2.2 m	2000 May 01	30.26	29.41	1.04
1992 QB_1	CKBO	Keck 10 m	1998 Nov 14	40.91	40.19	0.96
1993 SB.....	3:2	Keck 10 m	1998 Nov 15	31.05	30.3	1.28
1993 SC	3:2	Keck 10 m	1998 Nov 14	34.66	33.94	1.14
1994 TA	Centaur	Keck 10 m	1998 Nov 14	16.93	15.96	0.74
1994 TB	3:2	Keck 10 m	1998 Nov 15	30.08	29.48	1.51
1995 DA_2	4:3	Keck 10 m	1998 Nov 14	34.06	33.95	1.65
1995 WY_2	CKBO	Keck 10 m	1998 Nov 15	47.42	46.56	0.58
1995 WY_2	CKBO	Keck 10 m	1998 Nov 14	47.42	46.57	0.60
1996 RQ_{20}	CKBO	Keck 10 m	1998 Nov 15	39.46	38.70	0.91
1996 RR_{20}.....	3:2	Keck 10 m	1998 Nov 14	43.55	43.17	1.20
1996 SZ_4	3:2	Keck 10 m	1998 Nov 14	30.24	29.45	1.14
1996 TK_{66}	CKBO	Keck 10 m	1998 Nov 15	42.84	42.16	0.96
1996 TL_{66}	SKBO	Keck 10 m	1998 Nov 14	35.09	34.14	0.43
1996 TO_{66}	CKBO	Keck 10 m	1998 Nov 14	45.86	45.25	0.97
1996 TP_{66}	3:2	Keck 10 m	1998 Nov 14	26.39	25.49	0.93
1996 TQ_{66}	3:2	Keck 10 m	1998 Nov 15	34.61	33.70	0.65
1996 TS_{66}	CKBO	Keck 10 m	1998 Nov 15	38.82	37.87	0.37
1997 CQ_{29}	CKBO	Keck 10 m	1998 Nov 15	41.28	41.57	1.30
1997 CR_{29}.....	2:1?	Keck 10 m	1998 Nov 15	41.85	41.76	1.35
1997 CS_{29}	CKBO	Keck 10 m	1998 Nov 14	43.6	43.17	1.17
1997 CU_{26}	Centaur	Keck 10 m	1998 Nov 15	13.55	13.54	4.18
1997 CU_{29}	CKBO	Keck 10 m	1998 Nov 15	44.75	44.29	1.12
1997 QH_4	CKBO	Keck 10 m	1998 Nov 15	41.41	40.86	1.14
1997 QJ_4	3:2	Keck 10 m	1998 Nov 15	34.72	34.16	1.35
1998 SN_{165}.....	CKBO	Keck 10 m	1998 Nov 14	38.24	37.75	1.23
1999 DE_9.....	SKBO	UH 2.2 m	2000 Apr 28	33.81	33.78	1.54
1999 KR_{16}	CKBO	UH 2.2 m	2000 Apr 28	38.05	37.07	0.34
2000 EB_{173}	3:2	UH 2.2 m	2000 Jul 01	29.87	29.73	1.93

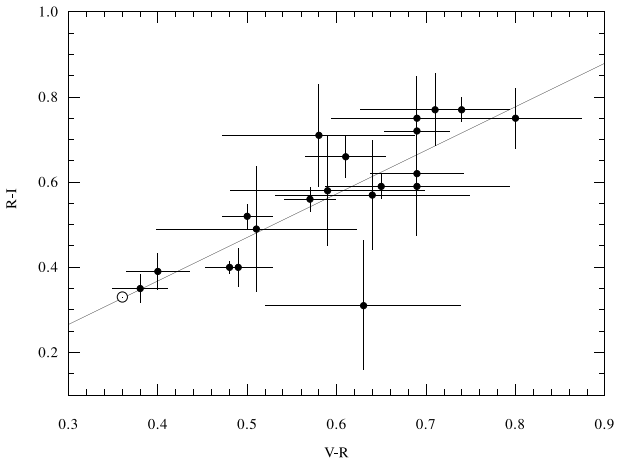

FIG. 4.—Plot of $V-R$ vs. $R-I$ for photometry from the present work having $\sigma_{B-V} < 0.15$ (see Table 2). The color of the Sun is marked.

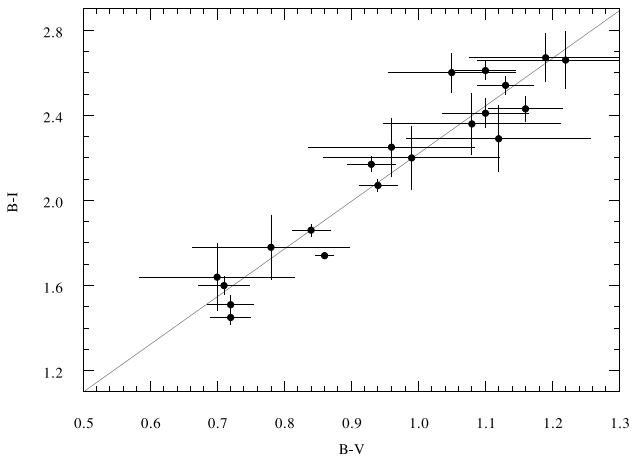

FIG. 5.—Plot of $B-V$ vs. $B-I$ for photometry from the present work having $\sigma_{B-V} < 0.15$ (see Table 2).

correlated with the optical gradients (Jewitt & Luu 1998; Davies et al. 2000). A subset of the complex hydrocarbons also mimic this property, notably some coal tar extracts studied by Cloutis et al. (1994) and the tholins (Cruikshank et al. 1998). The colors thus suggest, but do not uniquely diagnose, the presence of surface hydrocarbons.

The mean optical colors of the classical and resonant KBOs are indistinguishable (Table 4). The optical colors are correlated with neither the orbital nor the physical properties of the KBOs (Table 3). If collisional effects are important, we might expect a correlation between KBO color and ΔV, the difference between the average velocity and the velocity of an uninclined, circular orbit of the same semimajor axis. We computed ΔV from the eccentricity and inclination of each of the observed KBOs but find no statistically significant correlation with the $B-I$ color (Table 3). A $V-J$ versus semimajor axis correlation was tentatively claimed by Weintraub, Tegler, & Romanishin (1997), based on measurements of four Centaurs. In fact, this correlation is statistically insignificant [$P(N, r_{\rm corr}) < 0.1$] and is unsupported by the new data (Table 3).

Some of the objects in our sample have been previously

TABLE 2

OPTICAL PHOTOMETRY

Object	Date	$m_R(1,1,0)$ (mag)	R (mag)	$B-V$ (mag)	$V-R$ (mag)	$R-I$ (mag)
Pluto.....	2000 May 01	−1.37	13.42 ± 0.01	0.86 ± 0.01	0.48 ± 0.01	0.40 ± 0.01
1992 QB_1.....	1998 Nov 14	6.98	23.10 ± 0.09	0.99 ± 0.18	0.66 ± 0.15	0.80 ± 0.15
1993 SB.....	1998 Nov 15	7.91	22.83 ± 0.07	0.78 ± 0.12	0.51 ± 0.11	0.49 ± 0.15
1993 SC	1998 Nov 14	6.73	22.13 ± 0.04	1.05 ± 0.10	0.80 ± 0.07	0.75 ± 0.07
1994 TA	1998 Nov 14	11.25	23.44 ± 0.12	1.36 ± 0.29	0.62 ± 0.20	0.74 ± 0.21
1994 TB	1998 Nov 15	7.55	22.35 ± 0.05	1.19 ± 0.11	0.71 ± 0.08	0.77 ± 0.08
1995 DA_2	1998 Nov 14	8.13	23.51 ± 0.13	1.31 ± 0.27	0.51 ± 0.20	0.63 ± 0.24
1995 WY_2	1998 Nov 15	6.88	23.62 ± 0.14	1.03 ± 0.28	0.60 ± 0.23	0.51 ± 0.28
1995 WY_2	1998 Nov 14	6.95	23.69 ± 0.15	...	...	...
1996 RQ_{20}	1998 Nov 15	6.78	22.74 ± 0.07	0.96 ± 0.13	0.58 ± 0.11	0.71 ± 0.12
1996 RR_{20}.....	1998 Nov 14	6.72	23.14 ± 0.10	1.10 ± 0.21	0.69 ± 0.16	0.76 ± 0.16
1996 SZ_4	1998 Nov 14	8.34	23.13 ± 0.10	0.55 ± 0.15	0.61 ± 0.15	0.62 ± 0.17
1996 TK_{66}	1998 Nov 15	6.30	22.62 ± 0.06	1.08 ± 0.13	0.69 ± 0.10	0.59 ± 0.12
1996 TL_{66}	1998 Nov 14	5.04	20.45 ± 0.02	0.72 ± 0.03	0.38 ± 0.03	0.35 ± 0.03
1996 TO_{66}	1998 Nov 14	4.49	21.11 ± 0.03	0.72 ± 0.03	0.40 ± 0.04	0.39 ± 0.04
1996 TP_{66}	1998 Nov 14	6.85	21.03 ± 0.02	1.13 ± 0.04	0.69 ± 0.04	0.72 ± 0.04
1996 TQ_{66}	1998 Nov 15	7.17	22.53 ± 0.06	1.22 ± 0.13	0.69 ± 0.10	0.75 ± 0.10
1996 TS_{66}	1998 Nov 15	5.86	21.71 ± 0.03	1.10 ± 0.06	0.69 ± 0.05	0.62 ± 0.06
1997 CQ_{29}	1998 Nov 15	6.50	22.72 ± 0.07	0.99 ± 0.13	0.64 ± 0.11	0.57 ± 0.13
1997 CR_{29}.....	1998 Nov 15	7.04	23.31 ± 0.11	0.67 ± 0.20	0.69 ± 0.18	0.51 ± 0.22
1997 CS_{29}	1998 Nov 14	5.11	21.53 ± 0.03	1.16 ± 0.06	0.61 ± 0.05	0.66 ± 0.05
1997 CU_{26}	1998 Nov 15	6.39	17.87 ± 0.02	0.84 ± 0.03	0.50 ± 0.03	0.52 ± 0.03
1997 CU_{29}	1998 Nov 15	6.22	22.75 ± 0.07	1.12 ± 0.14	0.59 ± 0.11	0.58 ± 0.13
1997 QH_4	1998 Nov 15	6.88	23.07 ± 0.09	1.05 ± 0.18	0.65 ± 0.15	0.64 ± 0.16
1997 QJ_4	1998 Nov 15	7.31	22.73 ± 0.07	0.70 ± 0.12	0.63 ± 0.11	0.31 ± 0.15
1998 SN_{165}.....	1998 Nov 14	5.37	21.22 ± 0.03	0.71 ± 0.04	0.40 ± 0.04	0.40 ± 0.05
1999 DE_9.....	2000 Apr 28	4.68	20.04 ± 0.02	0.94 ± 0.03	0.57 ± 0.03	0.56 ± 0.03
1999 KR_{16}	2000 Apr 28	5.49	21.25 ± 0.02	1.10 ± 0.05	0.74 ± 0.03	0.77 ± 0.03
2000 EB_{173}.....	2000 Jul 01	4.61	19.43 ± 0.02	0.93 ± 0.04	0.65 ± 0.03	0.59 ± 0.03

TABLE 3

CORRELATIONS

Quantity[a]	Quantity[a]	N[b]	r_{corr}[c]	$P(r \geq r_{corr})$[d]
$B-I$.....	$V-J$	10	0.97	<0.001
$B-V$.....	$R-I$	28	0.70	<0.001
$V-R$.....	$R-I$	28	0.71	<0.001
$B-V$.....	$V-R$	27	0.44	0.02
$B-I$.....	$m_R(1,1,0)$	28	0.38	0.05
$B-I$.....	a	28	0.21	>0.1
$B-I$.....	e	28	0.30	>0.1
$B-I$.....	i	28	−0.08	>0.1
$B-I$.....	m_R	28	0.35	0.05
$B-I$.....	q	28	0.18	>0.1
$B-I$.....	R_h	28	0.02	>0.1
$B-I$.....	ΔV	28	0.19	>0.1

[a] $m_R(1,1,0)$ = red magnitude reduced to $R = \Delta = 1$ AU and to phase angle $\alpha = 0°$. a = semimajor axis, q = perihelion distance, R_h = heliocentric distance, ΔV = velocity relative to uninclined, circular Keplerian orbit.

[b] Number of measurements in the sample.

[c] Linear correlation coefficient.

[d] Probability that a larger correlation coefficient could be obtained by chance from N measurements of uncorrelated data. $P < 0.003$ indicates a correlation with $> 3\ \sigma$ significance.

measured. We compare the new results with published data in Table 5. A graphical comparison of the measurements is shown in Figure 7. In general, the independent measurements agree within the combined uncertainties. For example, five of 19 objects (26%) have independently measured $V-R$ colors that are different by more than one combined standard deviation (1 σ). This is consistent with a

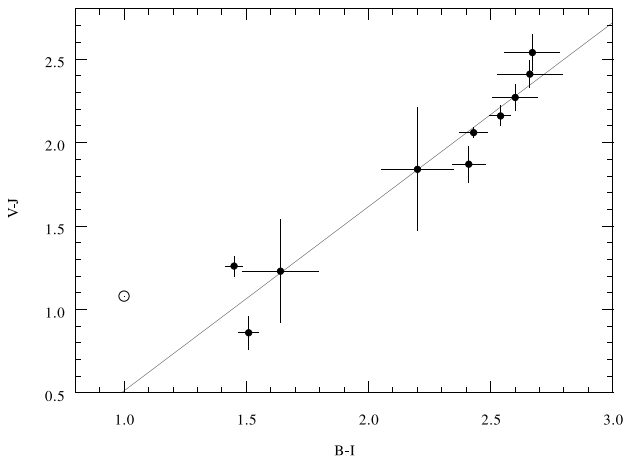

FIG. 6.—Plot of $B-I$ vs. $V-J$ for KBOs observed independently in the near-infrared by Jewitt & Luu (1998) and Davies et al. 2000.

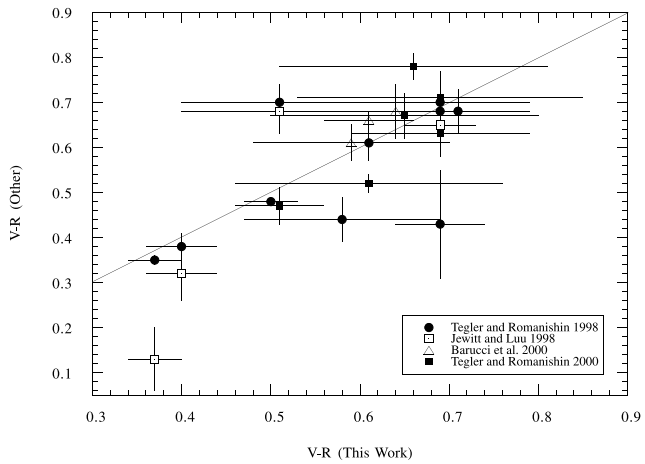

FIG. 7.—Comparison of the $V-R$ colors of KBOs measured in this work and reported independently. TR98 and TR00 are Tegler & Romanishin 1998 and 2000, respectively; JL98 is Jewitt & Luu 1998, while B00 is Barucci et al. 2000. The solid line is the track expected if the measurements are equal. Error bars have been suppressed for clarity; they may be read from Table 5.

Gaussian error distribution, for which we expect about 32% of measurements to lie beyond 1 σ. We summarize the data sets in Table 6. In terms of their extrema, means, and dispersions, the color samples of TR98, TR00, and the present work are remarkably concordant (cols. [3]–[5] in Table 6).

2.4. *The Color Distribution*

TR98 contend that the $B-V$ and $V-R$ colors are bimodally distributed. Their data, which include a mixture of Centaurs and KBOs, are plotted in Figure 8. In a later work Tegler & Romanishin (2000) reported observations of the $B-V$ and $V-R$ colors of 16 additional KBOs and three Centaurs (Fig. 9). They reported that the color distribution remained bimodal with the addition of the new data, although this is visually less obvious (compare Fig. 8 with Fig. 9). Tegler & Romanishin did not assess the statistical significance of the bimodality in either of their samples, and neither did they attempt to account for its physical origin. Clearly, a test of the significance of the reported bimodality is in order. We consider three such tests.

The bin test.—Most of the dispersion among the colors in Figures 8 and 9 occurs along a line of principal variation that is slightly inclined relative to the $B-V$ axis. We use the position of each KBO measured along this line, defined by

$$C = \sqrt{(B-V)^2 + (V-R)^2}\ , \qquad (6)$$

to test the null hypothesis that the colors are distributed randomly along the line. The probability that, in a sample of n measurements distributed randomly among k equal-

TABLE 4

COLOR MEANS

Sample[a]	N[b]	$B-V$[c]	$V-R$[c]	$R-I$[c]	$B-I$[c]
Classical.....	12	1.00 ± 0.04	0.61 ± 0.03	0.60 ± 0.04	2.22 ± 0.10
All resonant.....	12	0.96 ± 0.07	0.64 ± 0.03	0.61 ± 0.04	2.20 ± 0.12
3:2 only	10	0.95 ± 0.07	0.65 ± 0.03	0.62 ± 0.05	2.21 ± 0.14
All	28	0.98 ± 0.04	0.61 ± 0.02	0.60 ± 0.03	2.18 ± 0.07

[a] Dynamical subsample.

[b] Number of measurements in the subsample.

[c] Mean color and standard deviation on the mean.

TABLE 5

COMPARISON OF OPTICAL MEASUREMENTS

Object	Source	$m_R(1,1,0)$ (mag)	$B-V$ (mag)	$V-R$ (mag)	$R-I$ (mag)
1992 QB_1	This work	6.98 ± 0.09	0.99 ± 0.18	0.66 ± 0.15	0.80 ± 0.15
	TR00	6.92 ± 0.05	0.92 ± 0.06	0.78 ± 0.03	...
1993 SB	This work	7.91 ± 0.07	0.78 ± 0.12	0.51 ± 0.11	0.49 ± 0.15
	TR00	7.80 ± 0.04	0.82 ± 0.03	0.47 ± 0.04	...
1993 SC	This work	6.73 ± 0.04	1.05 ± 0.09	0.80 ± 0.07	0.75 ± 0.07
	LJ96	6.56 ± 0.05	0.92 ± 0.11	0.57 ± 0.09	0.86 ± 0.10
	DMG97	6.49 ± 0.10	...	0.54 ± 0.14	0.43 ± 0.14
	JL98	6.71 ± 0.02	0.94 ± 0.06	0.68 ± 0.05	0.68 ± 0.04
	TR98	...	1.27 ± 0.11	0.70 ± 0.04	...
1994 TB	This work	7.55 ± 0.05	1.19 ± 0.11	0.71 ± 0.08	0.77 ± 0.08
	TR98	...	1.10 ± 0.15	0.68 ± 0.06	...
1996 CU_{26}	This work	6.39 ± 0.02	0.84 ± 0.03	0.50 ± 0.03	0.52 ± 0.03
	TR98	...	0.77 ± 0.05	0.48 ± 0.01	...
	M99	6.18 ± 0.05	...	0.46 ± 0.02	0.56 ± 0.03
1996 RQ_{20}	This work	6.78 ± 0.07	0.96 ± 0.13	0.58 ± 0.11	0.71 ± 0.12
	TR98	...	...	0.44 ± 0.05	...
1996 RR_{20}	This work	6.72 ± 0.10	1.10 ± 0.21	0.69 ± 0.16	0.76 ± 0.16
	TR00	6.51 ± 0.03	1.16 ± 0.04	0.71 ± 0.03	...
1996 SZ_4	This work	8.34 ± 0.10	0.55 ± 0.15	0.61 ± 0.15	0.62 ± 0.17
	TR00	8.04 ± 0.04	0.83 ± 0.03	0.52 ± 0.02	...
1996 TK_{66}	This work	6.30 ± 0.06	1.08 ± 0.13	0.69 ± 0.10	0.59 ± 0.12
	TR00	6.21 ± 0.04	0.99 ± 0.02	0.63 ± 0.02	...
1996 TL_{66}	This work	5.04 ± 0.02	0.72 ± 0.03	0.37 ± 0.03	0.36 ± 0.04
	JL98	5.32 ± 0.04	0.58 ± 0.05	0.13 ± 0.07	0.54 ± 0.04
	TR98	...	0.75 ± 0.02	0.35 ± 0.01	...
1996 TO_{66}	This work	4.49 ± 0.03	0.72 ± 0.04	0.40 ± 0.04	0.39 ± 0.04
	JL98	4.52 ± 0.05	0.59 ± 0.06	0.32 ± 0.06	0.36 ± 0.07
	TR98	...	0.74 ± 0.04	0.38 ± 0.03	...
1996 TP_{66}	This work	6.85 ± 0.02	1.13 ± 0.04	0.69 ± 0.04	0.72 ± 0.04
	JL98	6.97 ± 0.04	0.80 ± 0.08	0.65 ± 0.07	0.69 ± 0.04
	TR98	...	1.17 ± 0.05	0.68 ± 0.03	...
1996 TQ_{66}	This work	7.17 ± 0.06	1.22 ± 0.13	0.69 ± 0.10	0.75 ± 0.10
	TR98	...	1.16 ± 0.10	0.70 ± 0.07	...
1996 TS_{66}	This work	5.86 ± 0.03	1.10 ± 0.06	0.69 ± 0.05	0.62 ± 0.06
	JL98	6.11 ± 0.08	0.93 ± 0.09	0.43 ± 0.12	0.67 ± 0.12
1997 CQ_{29}	This work	6.60 ± 0.07	0.99 ± 0.13	0.64 ± 0.11	0.57 ± 0.13
	B00	6.70 ± 0.05	0.99 ± 0.12	0.68 ± 0.06	0.62 ± 0.09
1997 CS_{29}	This work	5.11 ± 0.03	1.16 ± 0.05	0.61 ± 0.05	0.66 ± 0.05
	TR98	...	1.08 ± 0.07	0.61 ± 0.04	...
	B00	4.88 ± 0.02	1.05 ± 0.06	0.66 ± 0.02	0.53 ± 0.04
1997 CU_{29}	This work	6.22 ± 0.07	1.12 ± 0.14	0.59 ± 0.11	0.58 ± 0.13
	B00	6.16 ± 0.03	1.32 ± 0.12	0.61 ± 0.04	0.74 ± 0.06
1997 QH_4	This work	6.88 ± 0.09	1.05 ± 0.18	0.65 ± 0.15	0.64 ± 0.16
	TR00	6.88 ± 0.06	1.01 ± 0.07	0.67 ± 0.05	...
2000 EB_{173}	This work	4.61 ± 0.02	0.93 ± 0.04	0.65 ± 0.03	0.59 ± 0.03
	F01	4.72 ± 0.06	0.99 ± 0.14	0.60 ± 0.10	0.38 ± 0.09

NOTE.—References are as follows: B00 = Barucci et al. 2000; DMG97 = Davies, McBride, & Green 1997; F01 = Ferrin et al. 2001; LJ96 = Luu & Jewitt 1996; M99 = McBride et al. 1999; TR98 = Tegler & Romanishin 1998; TR00 = Tegler & Romanishin 2000.

sized bins, the central bin will hold m objects is given by

$$P(n, m) = \left[\frac{n!}{m!(n-m)!}\right] p^m (1-p)^{n-m}, \qquad (7)$$

where $p = 1/k$. We present calculations for three bins ($k = 3$) with C in the range $0.65 \leq C \leq 1.55$. Table 6 lists the number of objects in the central bin, which has $0.95 \leq C \leq 1.25$, for each sample.

Evaluation of the probabilities using equation (7) shows that the TR98 sample has roughly a 3% likelihood of having been drawn by chance from a uniform distribution, corresponding to a result that is $\approx 2.2\,\sigma$ in statistical significance. Tegler & Romanishin's larger second sample (TR00) is even less significantly bimodal (with a 13% probability of having been derived from a uniform distribution), as is the sample from the present work (for which the probability is also about 13% (Table 6). In fact, the combined TR98 + TR00 data sets are comparable to the data set from the present work in terms of size, range, mean, standard deviation on the mean, and the lack of evidence for a bimodal distribution of colors (Table 6). In all, we find that the data present a remarkably coherent case for a distribution of colors that is devoid of evidence for bimodality.

The bin test has been recomputed for other values of $C_{\min}$, $C_{\max}$, and k, but always with the results that (1) the

TABLE 6

RESULTS OF BIN TEST

Sample (1)	n[a] (2)	C_{min}[b] (3)	C_{max}[c] (4)	$C \pm \sigma_C$[d] (5)	m[e] (6)	$P(n,m)$[f] (7)	S[g] (8)
TR98	13	0.73	1.45	1.11 ± 0.08	1	0.033	0.967
TR00	19	0.80	1.41	1.14 ± 0.04	8	0.133	0.867
TR98 + TR00	32	0.73	1.45	1.13 ± 0.05	8	0.127	0.873
This work	28	0.81	1.49	1.16 ± 0.04	10	0.150	0.850

[a] Number of data points in the sample.
[b] Minimum value of color index.
[c] Maximum value of color index.
[d] Mean and standard deviation on the mean.
[e] Number of objects in central bin.
[f] Probability that m objects would be found in the central color bin from a sample of n objects drawn from a uniform distribution, from eq. (7).
[g] Statistical significance $S = 1 - P(n,m)$. Note that $S = 0.997$ corresponds to 3 σ confidence.

most significant (but still $< 3\ \sigma$) evidence for bimodality is in the TR98 data, and (2) the significance of bimodality decreases as the sample size increases. We conclude that the bin test provides no evidence that the $B-V$ or $V-R$ colors are distributed bimodally.

The dip test.—As another test for bimodality, we make use of the dip statistic (Hartigan & Hartigan 1985), which is defined as the maximum difference between the (perhaps bimodal) data distribution and the unimodal distribution function that minimizes that maximum difference. In effect, the test tries to explain the data distribution with a best-fitting unimodal distribution, and the dip statistic is the residual from matching the two functions. The larger the dip the larger the mismatch. Hartigan & Hartigan's test computes the dip statistic then evaluates its significance. The results upon performing the dip test on Tegler & Romanishin's data and our own data (this work) are presented in Table 7. In agreement with visual impressions (Fig. 8), the most nearly significant evidence for bimodality is in $V-R$ from TR98, but this is still less than 3 σ and not supported by the TR00 or present $V-R$ measurements. The dip test, like the bin test, provides no evidence in support of bimodality.

The interval distribution test.—We lastly consider the distribution of intervals between KBO color measurements. In a truly bimodal distribution, there should be a large interval (between modes) followed by many smaller intervals (between the members of each mode). Conversely, in a continuous distribution, one expects all intervals to be roughly equal. To assess the likelihood that the large interval observed in Tegler & Romanishin's color distribution might arise by chance from random, uncorrelated data, we computed Monte Carlo models in which we randomly picked colors from a uniform distribution, then determined the largest interval LI between two consecutive colors. We repeated this experiment 10^5 times in order to determine the probability of obtaining a given LI by random chance, given n data points. We selected colors in the ranges $0.60 \leq B-V \leq 1.30$ and $0.35 \leq V-R \leq 0.80$, respectively. For illustration, we present the results of our experiments in

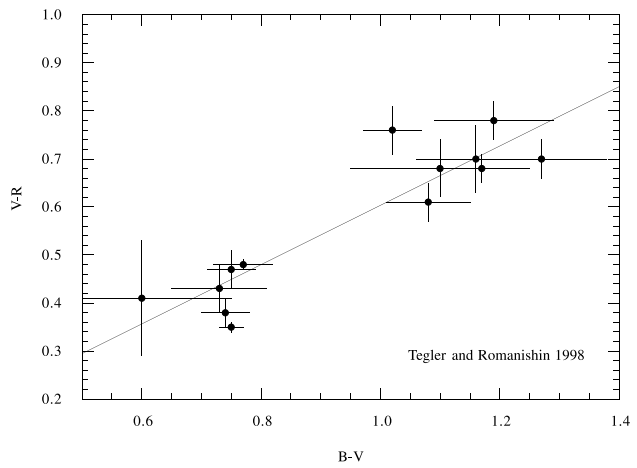

FIG. 8.—$B-V$ vs. $V-R$ from Tegler & Romanishin (1998)

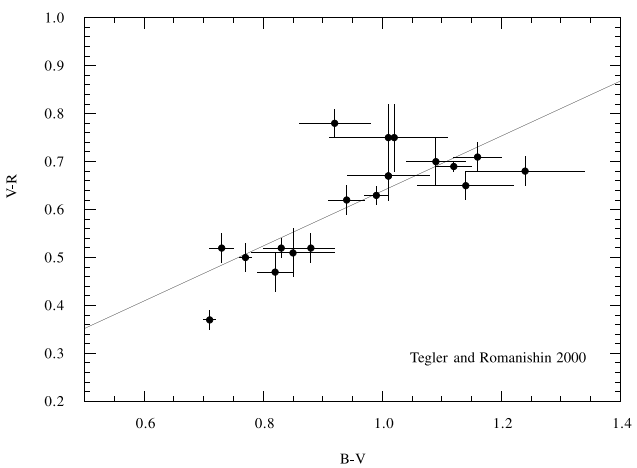

FIG. 9.—$B-V$ vs. $V-R$ from Tegler & Romanishin (2000)

TABLE 7

RESULTS OF DIP TEST

Sample	Color	n[a]	Dip Statistic	S[b]
TR98	$B-V$	13	0.13736	0.983
TR98	$V-R$	16	0.13542	0.993
TR00	$B-V$	19	0.05263	0.040
TR00	$V-R$	21	0.09921	0.933
This work	$B-V$	28	0.06766	0.584
This work	$V-R$	28	0.05555	0.239
This work	$R-I$	28	0.06790	0.597

[a] Number of data points.
[b] Statistical significance $S = 0.9970$ corresponds to the nominal 3 σ criterion for a statistically significant bimodality.

Figures 10 and 11, where we plot the LI cumulative probability distribution as a function of n for the $B-V$ and $V-R$ data sets.

The results of the interval distribution test are summarized in Table 8. There it can be seen that, at the canonical 3 σ ($P = 0.3\%$) level of confidence, the measured values of LI are consistent with random sampling of a uniform color distribution. This is already qualitatively obvious in a comparison of Figure 8 (TR98) with Figure 9 (TR00). The gap in Figure 9 is partially filled in relative to the gap in Figure 8, just as one expects from an enlarged data sample if the gap is merely a statistical fluctuation. A real gap in the color distribution would not shrink as the sample size increases.

We conclude that both our photometry and the photometry presented in two papers by Tegler & Romanishin are formally consistent with derivation from a uniform distribution of colors. Similarly, the distribution of optical-infrared ($V-J$) colors provides no hint of a bimodal distribution (Davies et al. 2000). These results are compatible with the original finding of Luu & Jewitt (1996) and with subsequent results presented by independent workers (Green et al. 1997; Barucci et al. 2000). Finding no significant evidence for bimodality, we next reconsider impact resurfacing as a possible cause of the observed unimodal color distribution.

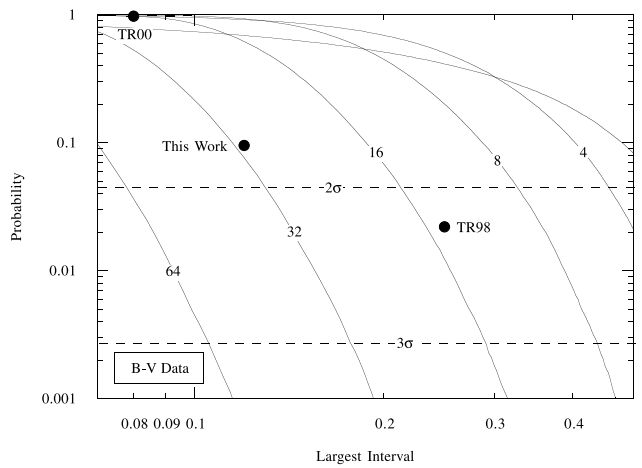

FIG. 10.—Probability of obtaining a largest interval (LI) greater than the one observed in a random sampling of a uniform distribution in $B-V$. The probabilities were calculated as described in the text. Solid lines are marked with the number of data points included in each simulation. Dashed lines mark 2 σ and 3 σ statistical confidence levels. Points show the observational samples.

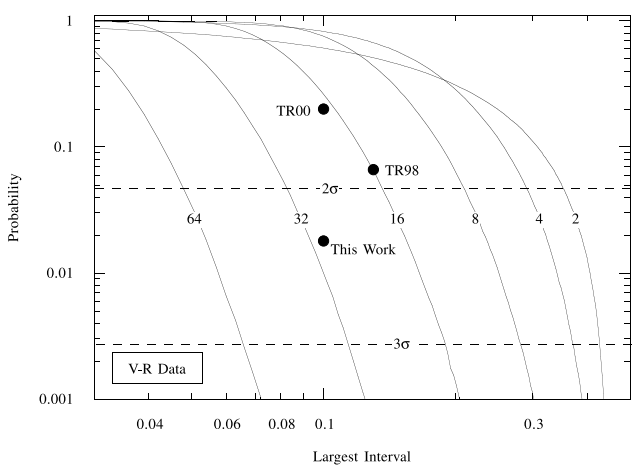

FIG. 11.—Same as Fig. 10 but for the $V-R$ color index

TABLE 8

RESULTS OF INTERVAL DISTRIBUTION TEST

Sample	Color	n[a]	LI_o[b]	$P(LI > LI_o)$[c]
TR98	$B-V$	13	0.25	0.012
TR98	$V-R$	16	0.13	0.062
TR00	$B-V$	19	0.08	0.974
TR00	$V-R$	21	0.10	0.245
This work.....	$B-V$	28	0.12	0.924
This work.....	$V-R$	28	0.10	0.990
This work.....	$R-I$	28	0.09	0.878

[a] Number of data points.
[b] Largest interval in the sample.
[c] Probability that a largest interval greater than the one observed would be produced by chance from data selected at random from a uniform distribution. $P = 0.003$ corresponds to the nominal 3 σ criterion for statistical significance.

3. RESURFACING REVISITED

We have revisited the resurfacing mechanism taking into account improvements in the known parameters of the KBO size distribution that have accrued from our Mauna Kea surveys (Jewitt, Luu, & Trujillo 1998; Trujillo et al. 2001). The most important change that has occurred since Luu & Jewitt (1996) is the improved determination of the size distribution index. The Kuiper belt objects are distributed such that the number of objects with radii in the range a to $a + da$ is $n(a)da = \Gamma a^{-q} da$, with Γ and q constant. The best-fit index $q = 4.0^{+0.6}_{-0.5}$ (Trujillo, Jewitt, & Luu 2001) is larger than the steepest models considered in Luu & Jewitt (1996). The total number of classical KBOs (CKBOs) larger than 100 km in diameter remains unchanged from our previous estimates at $N_{\rm CKBO} = 3.8^{+2.0}_{-1.5} \times 10^4$ (Trujillo et al. 2001).

The collision rate onto a target KBO of radius a_T is

$$1/\tau \approx \int_{a_{\rm min}}^{\infty} 4\pi(a_T + a)^2 \, \Delta V \psi n(a) da / W \, , \qquad (8)$$

where ΔV is the velocity difference between the target and incoming projectiles, ψ is a dimensionless factor for gravitational focussing, and W is the volume swept out by the orbits of the KBOs. Here $a_{\rm min}$ is the radius of the smallest projectile. In practice, the integration extends to the largest KBO in the distribution (not to infinity!) but, given the steep size distribution, impacts by the largest objects are comparatively rare and the integration upper limit is not critical. We take $\Delta V = 1.3$ km s^{-1} (Trujillo et al. 2001). The gravitational focussing is given by $\psi = 1 + (v_e/\Delta V)^2$, where v_e is the escape speed from the target object. For a spherical KBO of density ρ (kg m^{-3}), this may be expressed as

$$\psi = 1 + 8\pi G \rho a_T^2 / (3\Delta V^2) \qquad (9)$$

Substituting $\Delta V = 1.3$ km s^{-1}, $\rho = 10^3$ kg m^{-3}, we see that ψ differs from unity by no more than 10% for $a_T \leq 500$ km, meaning that we can safely set $\psi = 1$ for all the objects considered here. The classical Kuiper belt is well represented by an annulus with inner and outer radii, $R_i = 30$ AU, $R_o = 50$ AU, respectively, and thickness $H = 10$ AU, for which the volume is $W = \pi H(R_o^2 - R_i^2) = 2 \times 10^{38}$ m^3. With these parameters and with $q = 4$, $a_{\rm min} = 1$ km and

$a_T = 50$ km we obtain $1/\tau \approx 10^{-2}$ Myr^{-1} for objects in the classical Kuiper belt. The rate increases with decreasing projectile size (for example, with $a_{\rm min} = 0.1$ km, the corresponding rate is $1/\tau \approx 10^{1}$ Myr^{-1}), showing the importance of small impacts.

For the resurfacing model, we follow the prescription in Luu & Jewitt (1996). From equations (5)–(7) and (9) of that paper, the ejecta blanket radius is found to be

$$r_{\rm eb} = 17 \text{ km}(a/1 \text{ km})^{0.69}/(a_T/100 \text{ km})^{0.31} . \quad (10)$$

We again assume $q = 4.0$, noting that this index is determined for large KBOs ($a > 50$ km) and may not hold for the smaller objects that dominate collisional resurfacing. We computed Monte Carlo simulations for 1 Gyr at a time resolution of 1 Myr, using a 1000×1000 pixel array to represent the surface. Other important parameters include the timescale for radiation damage of the surface, which we take to be 10^8 yr (Luu & Jewitt 1996) and the minimum impactor size, for which we assumed a range of values $0.05 \leq a_{\rm min} \leq 1.0$ km. Sample models with $a_{\rm min} = 0.05$ km are shown in Figure 12.

The principal features of the data that we seek to compare with the resurfacing simulations are (1) the wide spread in the surface colors and (2) the absence of a measurable color-diameter trend. As noted in Luu & Jewitt (1996), steeper projectile size distributions increase the weight given to numerous small impacts relative to rare global resurfacing events. For this reason, the stochastic character of the new simulations is smaller than in Luu & Jewitt 1996. In fact, the $q = 4$, $a_T = 50$ km models show much less scatter than do the real KBOs (Fig. 12). In the observational sample the standard deviation on the mean of 28 measurements is $\sigma(V-R) = 0.02$ mag (Table 4), corresponding to 0.11 mag per object. The peak-to-peak color range in $V-R$ is 0.5 mag (Fig. 3). On the other hand, the resurfacing models typically give much more muted variations with peak-to-peak excursions less than 0.1 mag. Our first conclusion is that the color dispersion observed among the KBOs is larger than given by our $q = 4$ resurfacing model.

The resurfacing simulations predict a color-diameter trend, caused by the size dependence of the impact resurfacing time relative to the (constant) timescale for cosmic-ray irradiation damage of the surface (Fig. 12). The small KBOs are rapidly and repeatedly resurfaced, preventing them from reddening under the effects of cosmic rays whereas the large KBOs are difficult to resurface and therefore more susceptible to cosmic-ray irradiation. Small KBOs also display substantial color dispersion relative to the larger objects because the colors are less affected by spatial averaging. However, the color differences as a function of KBO size are modest. In the size domain of the observed objects, between $a_T = 50$ km and $a_T = 250$ km, the mean $V-R$ varies by only 0.1 mag (Fig. 12). A factor of 5 in radius corresponds, at constant albedo, to a 3.5 mag brightness difference. Inspection of the data shows that a 0.1/3.5 (mag/mag) color-magnitude gradient is too small to be seen in the real KBO sample, in view of the large intrinsic scatter. We conclude that the absence of a color-diameter trend in the KBO sample does not by itself constitute evidence against the action of resurfacing.

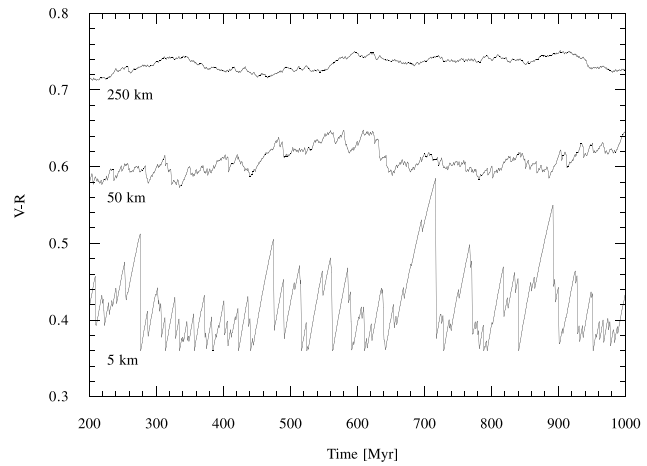

FIG. 12.—Sample resurfacing models computed as described in § 3. The curves show simulated color evolution on three KBOs having radii $a_T = 5$, 50, and 250 km (*bottom to top*). A $q = 4$ size distribution is used, as suggested by the observations, with a minimum projectile radius $a_{\rm min} = 0.05$ km. At the right we show the mean colors and the standard color deviations for each model.

Perhaps the least model-dependent and, therefore, most serious blow against the resurfacing hypothesis is its prediction that, for objects of a given diameter, azimuthal color variations should be equal in magnitude to the color dispersion among objects. That this is not the case among the real KBOs may be seen by inspection of Table 5. There, repeated determinations of the colors taken at random rotational phases are in general agreement within the quoted uncertainties of measurement while color differences between the KBOs are many times larger. The most significant exception is 1996 TL_{66}. Even here, however, the $V-R$ color range of 0.24 ± 0.08 mag. is small compared to the 0.5 mag. peak-to-peak color differences between objects (Tables 2 and 3). If resurfacing were the primary cause of the well-established color differences between KBOs, then rotational color variations from $V-R = 0.35$ to $V-R = 0.80$ would be seen in *individual* KBOs, and this is clearly not the case.

We conclude that impact resurfacing is probably not the primary cause of the color differences which exist among the KBOs. It remains possible that resurfacing plays a secondary role and may be responsible for azimuthal spectral variations like those reported on Centaur (8405) Asbolus (Kern et al. 2000). As noted in Luu & Jewitt (1996), resurfacing produces a range of colors only if the timescales for impact resurfacing and cosmic-ray reprocessing are of the same order. Neither timescale is easy to estimate. The irradiation timescale depends on the cross-section for interaction between the cosmic rays and the molecules comprising the KBO surface layers. This cross-section is highly composition dependent. The resurfacing timescale is dominated by the abundance of impactors which are too small to be detected in current surveys and whose statistics are therefore uncertain. Furthermore, impact gardening of KBO regoliths may be important in exposing previously buried material, as on the Moon, and modeling this effect introduces additional levels of arbitrariness. The net result is that we cannot argue, on physical grounds, that the relevant timescales are of the same order of magnitude, as is required for the hypothesis to succeed. Neither is it completely obvious that the color of an irradiated ice mixture changes with the fluence in the simple way assumed by the resurfacing hypothesis. Indeed, laboratory experiments show a more complicated relationship.

It is unlikely that simple grain size effects could be responsible for such a wide color diversity (Moroz et al.

1998). Instead, real compositional variations seem to be responsible. In the main (Mars–Jupiter) asteroid belt, some colorimetric diversity is produced by impact shattering of internally differentiated precursor bodies. This is not likely to be the explanation in the Kuiper belt, where the 100 km and larger objects studied here are too large to have been produced by fragmentation of precursors (Farinella & Davis 1996). As noted above, the compositional gradient in the main belt caused by a strong impressed radial temperature gradient is also unlikely to be relevant in the Kuiper belt, where temperatures are low and temperature differences are small. The primary origin of the color dispersion remains unknown.

3.1. *Other Reported Correlations*

Tegler & Romanishin (2000) reported that all nine observed KBOs with perihelia $q > 40$ AU systematically belong to their "red" group, while objects with smaller q are distributed more evenly between the red and grey groups. They showed that the probability of finding this result by random selection from a bimodal distribution is about 1/512, corresponding to about 3 σ in a Gaussian error distribution and argued that the effect is therefore of probable statistical significance.

We have reexamined Tegler & Romanishin's 1998 and 2000 data without making the classification of objects into "red" and "gray," since the data provide no support for this division. We use the $B-R$ color index as our metric, as this is more robust relative to measurement errors than either $B-V$ or $V-R$ separately. In their combined sample of 32 objects having $B-R$ color indices, there are 26 with $q < 40$ AU, for which the median value $(B-R)_m = 1.54$. All six objects with $q > 40$ AU have $B-R > (B-R)_m$. Given that the probability of any measurement falling above the median is, by definition, 1/2, the chance that all of six values would be larger than $(B-R)_m$ is $(1/2)^6 = 1/64$. The combined data sets from TR98, TR00 and this paper (Table 2) include 45 different objects with measured $B-R$ indices. We averaged separate measurements of multiply observed objects to obtain one $B-R$ per object. The median color for the 36 objects with $q < 40$ AU is $(B-R)_m = 1.46$, while all nine objects with $q > 40$ AU have $B-R > (B-R)_m$. If the $q > 40$ AU objects have the same median color as those with smaller perihelia, the probability of obtaining the observed result is $(1/2)^9 = 1/512$. We therefore concur with TR00 that there is statistical (≈ 3 σ) evidence for a color difference between objects having perihelia on either side of the $q = 40$ AU boundary. Clearly, however, this remains a weak result that should be tested by substantially increasing the sample size, particularly for objects with $q > 40$ AU. Until this is done, we see little point in speculating about possible causes of the color difference.

Levison & Stern (2001) reported a size dependence of the inclination distribution of KBOs, such that objects with absolute magnitude, $H < 6.5$ have a wider inclination distribution than others. However, using the Kolmogorov-Smirnov test, they find a 3% probability that the measured $H < 6.5$ and $H > 6.5$ distributions are drawn from the same parent population, corresponding to a result with 97% confidence. This, in turn, corresponds to about 2.2 σ in a Gaussian probability distribution and is therefore formally insignificant. Our own data show no evidence for a color-magnitude trend (Table 3) and no evidence that the $H < 6.5$ and $H > 6.5$ color distributions are different.

4. NEAR-INFRARED SPECTRA

Near-infrared spectral observations were obtained using the Keck I 10 m and the Subaru 8 m telescopes. At Keck we used the NIRC spectrometer (Matthews & Soifer 1994) at the f/25 forward Cassegrain focus. NIRC contains a 256×256 pixel InSb array with 30 μm pixels and a corresponding image scale of $0\farcs15$ pixel^{-1} ($38''$ FOV). A slit of projected dimensions $0\farcs68 \times 38''$ was used in conjunction with 150 line mm^{-1} and 120 line mm^{-1} grisms for the JH and HK spectral regions, respectively, giving spectral resolutions $\lambda/\Delta\lambda \approx 100$. Observations were taken in several steps. First, NIRC broadband images were used to identify the target KBOs by their motion relative to the fixed stars. Second, nonsidereal rates were entered into the telescope control system in order to follow the motion of the KBO. The telescope was moved while autoguiding to place the object at the slit location and the alignment was checked, iteratively, using further broadband images. Next, the slit and grism were inserted into the beam. A spectrum was taken while dithering the target image between two positions along the slit separated by $10''$. The alignment was rechecked every 20–30 minutes by removing the slit and reimaging the target. Spectral flat fields were obtained by imaging a diffusely illuminated spot inside the dome. Spectral calibration of the images was obtained from nearby stars on the UKIRT Faint Standards list (Hawarden et al. 2001). In addition, we observed nearby solar analogue stars in order to cancel features specific to the solar spectrum.

At the Subaru 8 m telescope we employed the CISCO camera in spectroscopic mode to acquire separate spectra in the JH and HK windows. CISCO is a high-throughput grating-dispersed near-infrared spectrometer using a 1024×1024 HgCdTe array of 18.5 μm pixels as detector (Motohara et al. 1998). The pixel scale is $0\farcs11$ pixel^{-1}, giving a $110'' \times 110''$ FOV. The spectral resolution was $\lambda/\Delta\lambda = 1000$. We identified the targets again through their proper motions. At the time of use, Subaru could not track at nonsidereal rates. For this reason, we observed 2000 EB_{173} near its stationary point to minimize the angular motion. As precautions, we used a relatively wide ($1\farcs0$) slit and we aligned the slit parallel to the apparent proper motion vector so that the natural motion of the object would carry it along, rather than out of the slit. As with NIRC, the alignment was periodically checked using broadband images and corrected when necessary. Flat fields were created from medians of the data. Calibration was again obtained using stars from Hawarden et al. 2001. The parameters of the spectral observations are listed in Table 9.

Spectral data reduction included steps to create and apply a bad pixel mask, flattening of the data, subtraction of night sky lines using adjacent dithered image pairs, removal of night sky line residuals by interpolation through the object position and, finally, extraction of the object spectrum. Variability in the transmission of the atmosphere, particularly in the water bands near 1.9 μm, also limit the photometric accuracy in some of the data. Fortunately, most observations were taken in dry atmospheric conditions and it was possible to take useful data through the atmospheric water absorption band. Nevertheless, systematic errors due to night sky lines and variable atmospheric extinction rival or dominate statistical errors in the spectra from NIRC. The higher resolution of the Subaru CISCO spectra allowed more accurate subtraction of the night sky

TABLE 9

OBSERVATIONAL PARAMETERS OF SPECTRA

UT Date	Instrument	Object	λ (μm)	Slit Width (arcsec)	$\lambda/\Delta\lambda$	Seeing (arcsec)	τ_{CSO}	Int[a] (s)
Keck I:								
1998 Nov 13	NIRC	1993 SC	*HK*	0.68	~100	0.6	0.06	6000
1998 Nov 13	NIRC	1996 TS_{66}	*JH*	0.68	~100	0.6–0.7	0.22	3600
1998 Nov 13	NIRC	1996 TS_{66}	*HK*	0.68	~100	0.6–0.7	0.22	3600
1999 Apr 3–4.....	NIRC	1999 DE_9	*JH*	0.68	~100	0.6	0.10–0.04	3000
1999 Apr 3–4.....	NIRC	1999 DE_9	*HK*	0.68	~100	0.6	0.10–0.04	6000
Subaru:								
2000 Jun 18	CISCO	2000 EB_{173}	*JH*	1.0	~1000	0.4	0.07	1440
2000 Jun 18	CISCO	2000 EB_{173}	*HK*	1.0	~1000	0.4	0.07	2880

[a] Accumulated integration time.

lines. The signal per resolution element in the CISCO data is very small, however, so that we must bin the data to obtain useful spectral information.

The reduced spectra are shown in Figures 13–17, where they have been divided by the spectrum of the Sun and normalized to unity at 2.2 μm. In Table 10 we list the normalized reflectivities binned to 0.1 μm resolution. Error bars on the binned points are 1 σ standard deviations on the means of the pixels within each bin. For each spectrum in Figures 13–17 we show the individual data points and overplot the binned data. We have included the spectrum of 1996 TL_{66} from Luu & Jewitt (1998) for comparison with

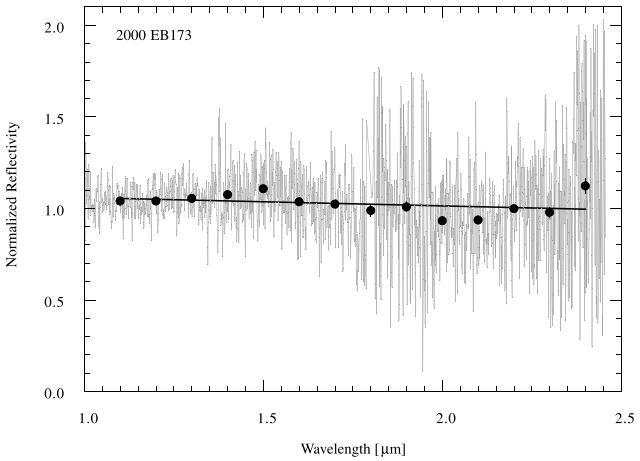

FIG. 13.—Reflection spectrum of 2000 EB_{173} taken with the Subaru telescope. The raw data are plotted in gray. The black circles denote the reflectivity binned to 0.1 μm resolution (see also Table 10). The solid line is a linear least-squares fit to the data.

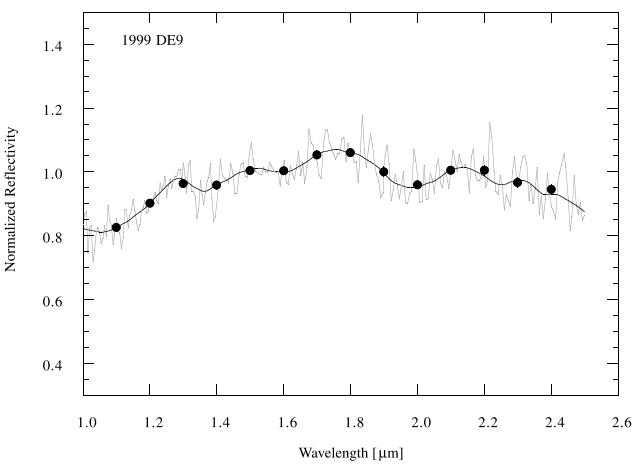

FIG. 14.—Reflection spectrum of 1999 DE_9 taken with the Keck telescope. The gray line shows the raw data. The black line through the data is a running mean added to guide the eye.

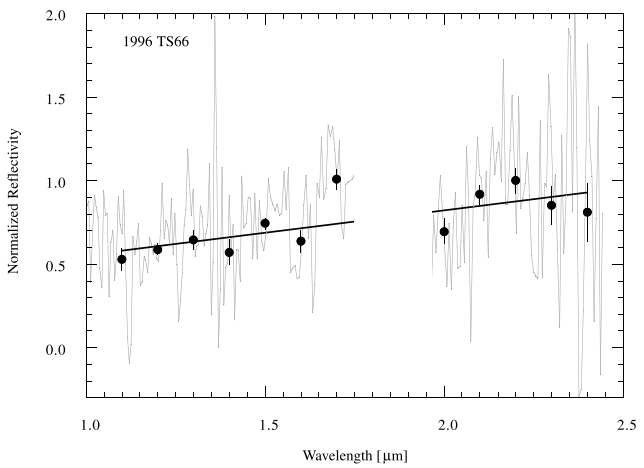

FIG. 15.—Reflection spectrum of 1996 TS66 taken with the Keck telescope. Individual pixels are plotted in gray. The black circles denote the reflectivity binned to 0.1 μm resolution (see also Table 10).

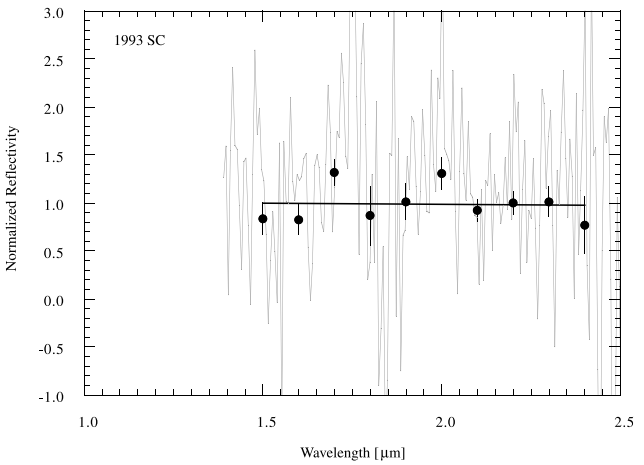

FIG. 16.—Same as Fig. 12 but for 1993 SC

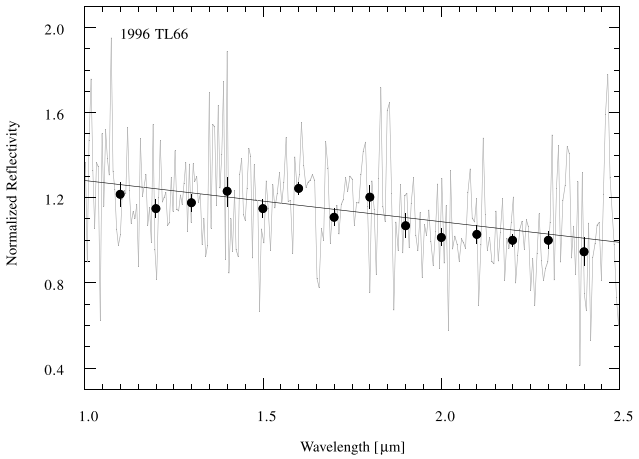

FIG. 17.—Same as Fig. 12 but for 1996 TL66 (from Jewitt & Luu 1998)

the new data. It was obtained at the Keck telescope using NIRC and observing procedures identical to those employed for the other KBOs.

4.1. *2000 EB_{173}*

Meaningful interpretation of the spectra demands a full understanding of systematic effects due to imperfect atmospheric extinction and sky line cancellation. These are best estimated empirically, by comparing spectra of standard stars taken at different times and air masses. The cleanest case is 2000 EB_{173} (Fig. 13), for which the night was dry and stable and the 1.9 μm telluric absorption feature is correspondingly well cancelled. The binned data suggest a broad absorption band centered near 2.0 μm, but, in view of the likely systematic uncertainties, we do not claim this feature as significant. We agree with Brown, Blake, & Kessler (2000), that the spectrum of 2000 EB_{173} is featureless in the $1.0 \leq \lambda \leq 2.5$ μm wavelength range. Unique compositional diagnoses of featureless spectra are obviously impossible. It is interesting to note, however, that laboratory reflection spectra of highly carbonized materials are commonly neutral and featureless, reflecting a deficiency of hydrogen bonds (Cloutis et al. 1994; Moroz et al. 1998). In the KBOs, we expect that hydrogen will be mobilized in the surface layers by continued cosmic-ray bombardment, leading to eventual escape and a net hydrogen depletion regardless of the initial composition.

4.2. *1999 DE_9*

In contrast, 1999 DE_9 is spectrally structured (Fig. 14). Absorption features are evident near 1.4, 1.6, 2.00, and (possibly) at 2.25 μm. The continuum drops from 1.3 μm down to the limit of the spectrum at 1.0 μm, which we interpret as an additional broad absorption centered at or shortward of 1.0 μm. Water ice has well-known features at 1.55, 1.65, and 2.02 μm. The 1.55 and 1.65 μm features appear very weakly in the DE_9 spectrum; we note this is a characteristic of spectra of fine grain frost (Clark 1981a). Water ice also has a high-overtone band at 1.25 μm, which is not seen in the DE_9 spectrum. The suppression of high-overtone bands relative to the low overtones (bands at longer wavelengths) is observed when other minerals are present in addition to water ice (Clark 1981a), and this might explain the absence of the 1.25 μm feature in 1999 DE_9. The strongest water band at 2.00 μm is only about 10% deep. The general weakness of the water ice features suggests a low abundance of water ice, or water ice that is heavily contaminated by an absorbing component. Indeed, the 1999 DE_9 spectrum is very similar to that of a mixture of Mauna Kea red cinder and 1% (by mass) water ice (Clark 1981b), shown in Figure 18. Notice that the $\approx$1.6 μm features in the cinder spectrum are extremely weak, as in 1999 DE_9, and that the $\approx$2.0 μm bands in the KBO and the Mauna Kea sample match in both position and width.

Features near 1.4 and 2.25 μm are usually diagnostic of the presence of metal-OH combination and overtone vibrational motions in minerals that incorporate OH within their crystal structure (Hunt 1977). The Mauna Kea spectrum in Figure 18 shows absorption near 1.4 μm and a probable band at 2.22–2.25 μm. The exact location of these bands can be diagnostic of the compound (either Al or Mg) associated with the OH stretch, but the quality of the DE9 spectrum is not good enough for us to make this identification. Given the limited spectral coverage and the unknown albedo, we tentatively assert that the spectrum of 1999 DE_9 shows evidence for the hydroxyl group, with the latter interacting with an Al or Mg compound. If it can be confirmed, the metal-hydroxyl identification would be most significant because the reactions that create the metal-OH compounds

TABLE 10

INFRARED REFLECTIVITIES

λ[a]	1999 DE_9	2000 EB_{173}	1996 TL_{66}	1996 TS_{66}	1993 SC
1.1.....	0.820 ± 0.009	1.040 ± 0.007	1.216 ± 0.054	0.529 ± 0.066	...
1.2.....	0.902 ± 0.010	1.040 ± 0.008	1.149 ± 0.041	0.587 ± 0.033	...
1.3.....	0.963 ± 0.011	1.053 ± 0.009	1.176 ± 0.041	0.645 ± 0.058	...
1.4.....	0.958 ± 0.013	1.075 ± 0.015	1.230 ± 0.068	0.570 ± 0.074	...
1.5.....	1.004 ± 0.010	1.107 ± 0.013	1.149 ± 0.041	0.744 ± 0.033	0.835 ± 0.165
1.6.....	1.003 ± 0.007	1.036 ± 0.014	1.243 ± 0.027	0.636 ± 0.066	0.824 ± 0.154
1.7.....	1.053 ± 0.013	1.023 ± 0.015	1.108 ± 0.041	1.008 ± 0.058	1.319 ± 0.132
1.8.....	1.060 ± 0.012	0.988 ± 0.034	1.203 ± 0.054	0.587 ± 0.107	0.868 ± 0.308
1.9.....	1.000 ± 0.017	1.007 ± 0.028	1.068 ± 0.054	0.496 ± 0.107	1.011 ± 0.187
2.0.....	0.959 ± 0.013	0.932 ± 0.021	1.014 ± 0.041	0.694 ± 0.074	1.308 ± 0.165
2.1.....	1.005 ± 0.009	0.936 ± 0.015	1.027 ± 0.041	0.917 ± 0.058	0.923 ± 0.110
2.2.....	1.000 ± 0.016	1.000 ± 0.018	1.000 ± 0.027	1.000 ± 0.074	1.000 ± 0.121
2.3.....	0.967 ± 0.015	0.978 ± 0.026	1.000 ± 0.041	0.851 ± 0.116	1.011 ± 0.154
2.4.....	0.945 ± 0.017	1.122 ± 0.040	0.946 ± 0.068	0.810 ± 0.174	0.769 ± 0.297

[a] Central wavelength of the bin (μm).

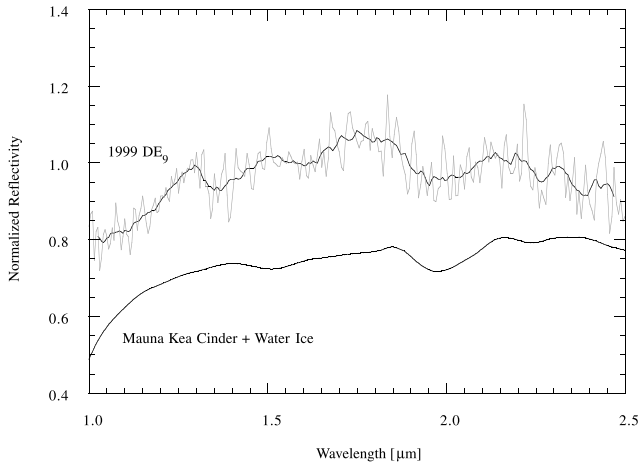

FIG. 18.—Reflection spectrum of 1999 DE_9 compared with a Mauna Kea cinder plus 1% water ice (by weight) sample from Clark 1981b. The 1999 DE_9 spectrum is shown unsmoothed (*gray line*) and running-box smoothed by 0.05 μm (*black line*). The Mauna Kea spectrum has been vertically offset for clarity.

proceed only in the presence of liquid water, implying that temperatures near the melting point have been sustained in 1999 DE_9 for at least a short period of time. Localized impacts on surface materials on 1999 DE_9 might provide a sufficient (although transient) heat source. Heating of core volatiles by the prolonged decay of radioactive elements could also lead to melting but a mechanism of transport to the surface would in addition be required for these materials to be spectrally observable.

A similar absorption near 2.27 μm is present in the spectrum of Centaur (5145) Pholus (Davies, Sykes, & Cruikshank 1993; Luu, Jewitt, & Cloutis 1994), with which 1999 DE_9 shares a resemblance in the $1.4 < \lambda < 2.4$ μm wavelength range (Fig. 19). This feature has been tentatively interpreted as due to solid methanol (CH_3OH; Cruikshank et al. 1998). However, as Cruikshank et al. note, the identification with methanol is uncertain in part because an expected second band at 2.33 μm is not observed. The Pholus spectrum modeled by these authors has an unfortunate gap at 1.4 μm. We recommend that this wavelength be observed to search for evidence for the counterpart metal-OH absorption feature suspected in 1999 DE_9.

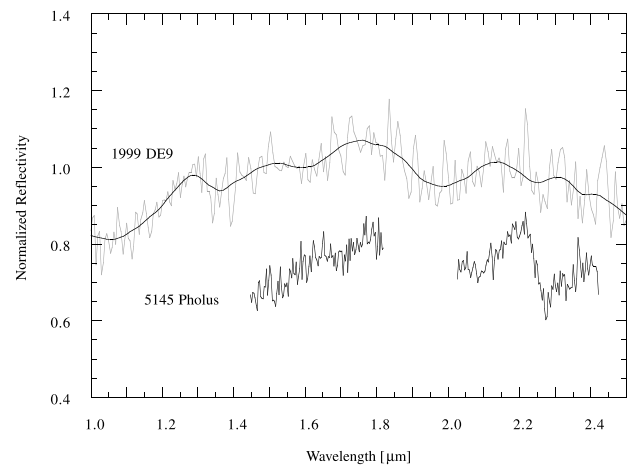

FIG. 19.—Reflection spectrum of 1999 DE_9 compared with the spectrum of Centaur (5145) Pholus (from Luu et al. 1994). The 1999 DE_9 spectrum is shown unsmoothed (*gray line*) and running-box smoothed by 0.05 μm (*black line*). The (5145) Pholus spectrum has been vertically offset for clarity.

Lastly, our spectrum of 1999 DE_9 shows a broad absorption in the 1.0 μm $< \lambda <$ 1.3 μm wavelength region with an apparent minimum near 1.05 μm. Unfortunately, the minimum is close to the short wavelength end of our spectrum, and we cannot be confident of the trend of the reflectivity at $\lambda \leq 1.0$ μm. A true minimum near this wavelength would be suggestive of the presence of a ferrous silicate, possibly an olivine (Cloutis & Gaffey 1991). Forsterite (Mg_2SiO_4, a magnesium-rich olivine) has been independently proposed to fit a 1 μm absorption in the reflection spectrum of Centaur (5145) Pholus (Cruikshank et al. 1998) and would fit the 1 μm absorption in 1999 DE_9. The identification of Forsterite as the specific form of silicate is nonunique, but it is attractive because of the known presence of Forsterite in the dust ejected from comets (Crovisier et al. 2000). The single object 1999 DE_9 thus provides plausible compositional ties to both the Centaurs and the nuclei of comets (which are known to be water-rich) through the water ice (Foster et al. 1999; McBride et al. 1999; Luu, Jewitt, & Trujillo 2000) and silicate (Cruikshank et al. 1998) bands. On the other hand, if the reflectivity continues to decline at $\lambda \leq 1.0$ μm, we would instead suspect that the absorption is due to the same complex hydrocarbons (e.g., tholins) that give reddish optical colors to the KBOs. Only new spectra will allow us to decide between these interpretations.

4.3. *1993 SC*

Numerous absorptions were reported in the near-infrared spectrum of 1993 SC by Brown et al. (1997). Their spectrum was taken at Keck with the NIRC spectrometer over a range of air masses from 1.2 to 1.7 and with an integration time of 3600 s. They reported absorption features at 1.62, 1.79, 1.95, 2.20, and 2.32 μm, with depths up to 50% of the local continuum. The features were not precisely identified by Brown et al., but a broad classification as hydrocarbon absorptions was made. We targeted the $H-K$ spectral region of 1993 SC specifically to examine the features reported by Brown et al. Our integration of 6000 s was recorded between air masses 1.04 and 1.09, with sky cancellation using a nearby star observed at air mass 1.08.

None of the features reported by Brown et al. are apparent in our data. Instead, using the same instrument on the same telescope but with a longer integration time, we find only a noisy continuum devoid of significant spectral structure (Fig. 16). In our spectrum, the reflectivity in the 2.25–2.35 μm bin is 1.01 ± 0.15. This is incompatible with Brown et al.'s deepest minimum at 2.32 μm at the 3.3 σ level. (Brown et al. presented their data heavily smoothed by convolution with a Gaussian, which impedes a more detailed comparison with the unsmoothed data in Fig. 16.) Simple experiments in which our data were smoothed by convolution with a Gaussian generated (apparently deep but unreal) features with wavelengths that did not match those reported by Brown et al. As another metric of comparison, we compute $S_{2.2}/S_{1.6}$, the ratio of the reflectivity at K band ($S_{2.2}$) to that at H band ($S_{1.6}$). In the Brown et al. spectrum this ratio is $S_{2.2}/S_{1.6} = 2.2$ (see their Fig. 1), while we measure $S_{2.2}/S_{1.6} = 1.0 \pm 0.1$ (Fig. 16). Finally, earlier broadband photometry gives $H-K = -0.04 \pm 0.19$ (Jewitt & Luu 1998), which, with the solar $H-K = 0.06$,

corresponds to $S_{2.2}/S_{1.6} = 0.91 \pm 0.19$. The filter photometry and our new spectrum are mutually consistent, but do not support the much larger $S_{2.2}/S_{1.6}$ of Brown et al. We have no explanation for the differences between our spectrum and that of Brown et al.

4.4. *Discussion*

We also obtained spectra of 1996 TL_{66} (Fig. 17, taken from Luu & Jewitt 1998) and 1996 TS_{66} (Fig. 15). When considered with the spectrum of 1996 TO_{66} (Brown, Cruikshank, & Pendleton 1999) we see a remarkable diversity of spectral characteristics among the KBOs. Some (2000 EB_{173}, 1996 TL_{66}, 1996 TS_{66}, and 1993 SC) appear spectrally bland at the achievable signal-to-noise ratios. Others (1996 TO_{66}, 1999 DE_9) show absorptions due to water ice. The remarkable 1999 DE_9 shows additional evidence for absorption near 1 μm that may indicate surface olivines and weaker bands as discussed above.

What do these spectral differences mean? There is no obvious correlation with the optical colors (e.g., $B-I$, Table 2) or absolute magnitudes. Indeed, it is too early to detect patterns in the spectral properties of the bodies in the outer solar system. An enlarged sample of high-quality spectra is needed, which will require long integrations on the brightest KBOs with the largest telescopes. Parallel measurements of the albedos using simultaneous optical and thermal measurements (presumably from the SIRTF spacecraft but perhaps also from ground-based submillimeter telescopes) are also needed to better understand the compositions of the KBOs.

The Centaurs and the nuclei of the Jupiter-family comets probably share a common origin in the Kuiper belt. Spectral observations of these objects should show a diversity parallel to that seen among the KBOs. Indeed, near-infrared spectra of the Centaurs (2060) Chiron and (5145) Pholus show, respectively, neutral near-infrared continuum with superposed water ice bands, but no other features (Foster et al. 1999; Luu et al. 2000), and a structured continuum with evidence for olivine, a low-mass hydrocarbon (possibly methanol), as well as water (Cruikshank et al. 1998). Qualitatively, at least, these two Centaurs are analogues of Kuiper belt objects 1996 TO_{66} (Brown et al. 1999) and 1999 DE_9 (Fig. 14), respectively. Spectra of more Centaurs are urgently needed. Recent estimates predict that 20–30 Centaurs should have $m_R < 20$ and thus be within range of spectral investigation with the largest telescopes (Fig. 4 of Sheppard et al. 2000). The nuclei of comets present an even more difficult observational challenge. They are small and tend to be surrounded by dust comae when close to the Sun and bright enough to be studied. Despite this, obtaining nucleus spectra should be a high scientific priority for those interested in the origin of the comets and the nature of the Kuiper belt.

5. SUMMARY

We present new optical photometry and near-infrared spectra of Kuiper belt objects, taken to study the spectral diversity among these bodies and to search for physically revealing correlations. We find that:

1. The optical ($B-V$, $V-R$ and $R-I$) and optical to near-infrared ($V-J$) colors of KBOs show a dispersion that is large compared to the uncertainties of measurement. The color indices are mutually correlated, indicating the ubiquitous presence of a single reddening agent in the 0.45 to 1.2 μm wavelength range.
2. There is no statistically significant (3 σ) evidence for a bimodal distribution of the $B-V$ versus $V-R$ colors, either in our sample or in the observations reported by Tegler & Romanishin (1998, 2000).
3. The colors are not linearly correlated with any orbital or known physical properties of the KBOs. Specifically, we find no linear correlation of the optical color indices with heliocentric distance, orbital semimajor axis, inclination, eccentricity, circular velocity difference or absolute magnitude. However, at the 3 σ confidence level, we do confirm Tegler & Romanishin's (2000) finding that objects with perihelia $q > 40$ AU are systematically redder than others. The mean colors of the classical and resonant Kuiper belt objects are indistinguishable.
4. Impact resurfacing (Luu & Jewitt 1996) is probably not the primary cause of the color dispersion among KBOs, for two reasons. First, the color dispersion among KBOs is larger than can be easily produced in Monte Carlo models of the resurfacing process. Second, the resurfacing hypothesis predicts that, in a statistical sense, individual objects should show azimuthal color variations as large as the color differences between objects. The measurements show that this is not the case.
5. The KBOs are also spectrally diverse in the near-infrared, from featureless to continua marked by distinct solid state absorptions. In particular, 1999 DE_9 shows remarkable similarity to the spectrum of a Mauna Kea cinder plus water ice mixture, with a water ice feature near 2.0 μm and depression of the continuum at $\lambda \leq 1.3$ μm that is consistent with (but not uniquely diagnostic of) olivine absorption.
6. Our 1.4–2.4 μm reflection spectrum of 1993 SC shows no evidence of the existence of absorption features reported by Brown et al. (1997). Furthermore, the spectral slope reported by Brown et al. is inconsistent with the spectral slope measured here, and with independent broadband photometry.

We thank Wayne Wack, Gary Punawai, and John Dvorak for their observing assistance and Support Scientists Ken Motohara and Bob Goodrich for their help with the setups. Chad Trujillo and Scott Sheppard helped with some of the observations. Ted Roush and Ed Cloutis gave helpful comments on our spectrum of 1999 DE_9. John Davies provided a prompt review. We thank Jan Kleyna and Jing Li for discussions about statistics and we gratefully acknowledge support from NASA's Origins Program.

REFERENCES

Barucci, M. A., Fulchignoni, M., Birlan, M., Doressoundiram, A., Romon, J., & Boehnhardt, H. 2001, A&A, 371, 1150
Barucci, M. A., Romon, J., Doressoundiram, A., & Tholen, D. 2000, AJ, 120, 496
Brown, M., Blake, G., & Kessler, J. 2000, ApJ, 543, L163
Brown, R., Cruikshank, D., & Pendleton, Y. 1999, ApJ, 519, L101
Brown, R., Cruikshank, D., Pendleton, Y., & Veeder, G. 1997, Science, 276, 937
Clark, R. N. 1981a, J. Geophys. Res., 86, 3087
———. 1981b, J. Geophys. Res., 86, 3074
Cloutis, E., & Gaffey, M. J. 1991, J. Geophys. Res., 96, 22809
Cloutis, E., Gaffey, M., & Moslow, T. 1994, Icarus, 107, 276

Crovisier, J., et al. 2000, in ASP Conf. Ser., 196, Thermal Emission Spectroscopy and Analysis of Dust, Disks, and Regoliths, ed. M. Sitko, A. Sprague, & D. Lynch (San Francisco: ASP), 109
Cruikshank, D., et al. 1998, Icarus, 135, 389
Davies, J. K., Green, S., McBride, N., Muzzerall, E., Tholen, D. J., Whiteley, R. J., Foster, M. J., & Hillier, J. K. 2000, Icarus, 146, 253
Davies, J. K., McBride, N., & Green, S. F. 1997, Icarus, 125, 61
Davies, J. K., Sykes, M., & Cruikshank, D. 1993, Icarus, 102, 166
Ferrin, I., et al. 2001, ApJ, 548, L243
Farinella, P., & Davis, D. R. 1996, Science, 273, 938
Foster, M., Green, S., McBride, N., & Davies, J. 1999, Icarus, 141, 408
Green, S., McBride, O'Ceallaigh, D., Fitzsimmons, A., Williams, I., & Irwin, M. 1997, MNRAS, 290, 186
Hartigan, J. A., & Hartigan, P. M. 1985, Ann. Stat., 13, 70
Hartmann, W., Cruikshank, D., & Degewij, J. 1982, Icarus, 52, 377
Hartmann, W., Tholen, D., Meech, K., & Cruikshank, D. 1990, Icarus, 83, 1
Hawarden, T., Leggett, S. K., Letawsky, M., Ballantyne, D., & Casali, M. 2001, MNRAS, 325, 563
Hunt, G. R. 1977, J. Geophys., 42, 501
Jewitt, D. C., & Luu, J. X. 1998, AJ, 115, 1667
Jewitt, D. C., Luu, J., & Chen, J. 1996, AJ, 112, 1225
Jewitt, D. C., Luu, J., & Trujillo, C. 1998, AJ, 115, 2125
Kern, S., McCarthy, D., Buie, M., Brown, R., Campins, H., & Rieke, M. 2000, ApJ, 542, L155
Landolt, A. 1992, AJ, 104, 340
Levison, H., & Stern, S. A. 2001, AJ, 121, 1730
Luu, J. X., & Jewitt, D. C. 1996, AJ, 112, 2310
———. 1998, ApJ, 494, L117
Luu, J. X., Jewitt, D. C., & Cloutis, E. 1994, Icarus, 109, 133
Luu, J. X., Jewitt, D. C., & Trujillo, D. C. 2000, ApJ, 531, L151
Luu, J., Marsden, B., Jewitt, D., Trujillo, Hergenrother, C., Chen, J., & Offutt, W. 1997, Nature, 387, 573
Matthews, K., & Soifer, B. T. 1994, in Infrared Astronomy with Arrays: The Next Generation, ed. I. McLean (Dordrecht: Kluwer), 239
McBride, N., Davies, J., Green, S., & Foster, M. 1999, MNRAS, 306, 799
Moroz, L., Arnold, G., Korochantsev, A., & Wasch, R. 1998, Icarus, 134, 253
Motohara, K., et al. 1998, Proc. SPIE, 3354, 659
Noll, K. S., Luu, J., & Gilmore, D. 2000, AJ, 119, 970
Oke, J., et al. 1995, PASP, 107, 375
Sheppard, S., Jewitt, D., Trujillo, C., Brown, M., & Ashley, M. 2000, AJ, 120, 2687
Tegler, S. C., & Romanishin, W. 1998, Nature, 392, 49
———. 2000, Nature, 407, 979
Trujillo, C., Jewitt, D., & Luu, J. 2000, ApJ, 529, L103
———. 2001, AJ, 122, 457
Weintraub, D., Tegler, S., & Romanishin, W. 1997, Icarus, 128, 456